Rare Metal Materials and Engineering
Volume 51, Issue 6, June 2022
Available online at www.rmme.ac.cn

Science Press

Cite this article as: Xue Hansong, Zhou Yang, Li He, et al. Effect of Minor Gd Addition on Microstructure Evolution and Properties of As-cast Mg-8Zn-1Mn-3Sn Alloy[J]. Rare Metal Materials and Engineering, 2022, 51(06): 2011-2019.

ARTICLE

Effect of Minor Gd Addition on Microstructure Evolution and Properties of As-cast Mg-8Zn-1Mn-3Sn Alloy

Xue Hansong[1,2], Zhou Yang[1], Li He[1], Wang Jinyang[1], Liu Song[1], Zhang Dingfei[2]

[1] College of Materials Science and Engineering, Chongqing University, Chongqing 400044, China; [2] National Engineering Research Center for Magnesium Alloys, Chongqing University, Chongqing 400044, China

Abstract: The effect of minor Gd element on the microstructure and properties of Mg-8Zn-1Mn-3Sn alloy was studied. The results show that Mg-8Zn-1Mn-3Sn-*x*Gd is mainly composed of α-Mg matrix, $MgZn_2$, MgZn, Mg_7Zn_3, Mg_2Sn phase and MgSnGd phase. The MgSnGd phase is a high temperature phase, which is formed firstly during the solidification and changes the solidification process, causing the semi-continuous second phase at the grain boundary to transform into a discontinuous network. The MgSnGd phase has a coherent orientation relationship with the α-Mg matrix, which can be used as a heterogeneous nucleation core to refine grains. The Mg-8Zn-1Mn-3Sn-0.5Gd alloy has the best comprehensive mechanical properties. The mechanical properties of the alloy are significantly improved by adding Gd elements to refine the grains, and the MgSnGd phase pins the grain boundary to hinder the movement of dislocations and the transformation of the second phase of the grain boundary.

Key words: Mg-Zn-Mn-Sn alloy; MgSnGd phase; grain refinement; mechanical properties; Gd addition

As the lightest structural metal material, magnesium alloy is widely used in automobile, aerospace and other fields due to its high specific strength and good casting performance[1-3]. Mg-Zn-Mn alloy has high tensile strength, low production cost, and excellent thermal processing performance. As a low-cost alloying element, Sn element can not only refine the grains after being added to the alloy, but also can form the stable Mg_2Sn phase (770 °C) which precipitates at the grain boundary, pins the grain boundary to hinder the movement of dislocations and thus enhances the strength of the alloy[4]. According to the previous research of our group, the tensile strength and yield strength of the extruded Mg-6Zn-1Mn alloy increase from 310 MPa to 328 MPa, and from 210 MPa to 255 MPa after adding 4wt% Sn, respectively[5]. However, its absolute strength is low, which restricts its wide application to a certain extent, so it is necessary to further improve the ultimate tensile strength and plasticity of the alloy.

Alloying, as an effective method to improve the mechanical properties of alloys, is widely used in the research of magnesium alloy modification[6-8]. According to related research[9-13], Ce, Y, Nd, Gd elements are added to Mg-Zn-Mn alloy, which can further improve the mechanical properties of the alloy. Among the above alloying elements, Gd has the most similar lattice parameters to Mg and a larger solid solubility in magnesium (23.49wt% at 548 °C)[14]. Therefore, adding high content of Gd (usually greater than 10wt%) has a better solid solution strengthening effect and can effectively improve the comprehensive mechanical properties of the alloy. For instance, Xu[15] studied the effect of Gd on the hardness and tensile strength of magnesium alloys, and the results showed that the hardness and tensile strength of the alloy increase linearly with the increase of Gd content. At present, most of the research adds high content of Gd element to form a long-period stacking ordered structure Mg-Zn-Gd phase to improve the mechanical properties of the alloy[16,17]. There are few studies on the effect of minor Gd on the microstructure and mechanical properties of magnesium alloys. In addition, the addition of RE element to the Mg-Zn-Mn-Sn alloy can not only precipitate the strengthening phase $\beta'(MgZn_2)$, but also generate the MgSnRE phase, which can

Received date: June 19, 2021
Foundation item: National Great Engineering Research Project of China (2016YFB0301101); Chongqing Technology Innovation and Application Development Special Project (cstc2019jscx-mbdxX0033)
Corresponding author: Xue Hansong, Ph. D., Associate Professor, College of Materials Science and Engineering, Chongqing University, Chongqing 400044, P. R. China, Tel: 0086-23-65111212, E-mail: hsxue@sohu.com

realize the effect of multi-phase strengthening. Hu[18,19] studied the effect of RE element (Nd, Y) on the microstructure and mechanical properties of Mg-Zn-Mn-Sn alloys. The results showed that MgSnNd and MgSnY are high-temperature phases that can promote the age hardening response of the heat-treated alloys. Our research group previously studied the effect of Gd on the structure and age hardening behavior of Mg-6Zn-1Mn-4Sn alloy[20]. The results show that the MgSnGd phase can be formed with the addition of Gd. At the same time, trace Gd can increase the peak hardness and shorten the peak aging time, while excessive Gd will weaken the age hardening response. However, the formation mechanism of MgSnGd phase during the solidification process has seldom been studied. Meanwhile, there are few related studies on the mechanism of modifying the microstructures and enhancing the mechanical properties of the alloy owing to the formation of MgSnGd phase.

In this study, a Mg-8Zn-1Mn-3Sn (ZMT813) alloy was used as the basic alloy, and minor Gd element was added to the alloy. The effect of minor Gd on the microstructure evolution and properties of Mg-8Zn-1Mn-3Sn as-cast alloy was studied by optical microscope (OM), scanning electron microscope (SEM), X-ray diffractometer (XRD), energy spectrometer (EDS), field emission-electron probe micro-analyzer (FE-EPMA), and differential scanning calorimeter (DSC). At the same time, the morphology change mechanism of MgSnGd phase was also studied.

1 Experiment

In this experiment, four groups of alloys with different compositions were designed. The raw materials were pure magnesium ingot (99.99wt%), pure zinc particles (99.99wt%), Sn particles (99.99wt%), Mg-2.7wt% Mn master alloy, and Mg-30wt% Gd master alloy. The melting experiment was conducted in a pit-type crucible resistance furnace. The melts were held at 750 °C for 20 min. Then the melts were poured into a mold crucible (preheated at 250 °C). The protective gas (99%CO_2+1%SF_6) was used to prevent oxidation during melting and pouring. The chemical composition of the alloy was designed and reported in Table 1. The CMTG5105 universal testing machine was used to test the mechanical properties of the alloy. The stretched sample was cut into a size of 14 mm×6 mm×2 mm (Fig.1). The mechanical property test was room temperature stretching, and the stretching speed was 2 mm/min. The samples used for microstructure observation were polished with metallographic sandpaper, and then the samples were etched with 5% nitric acid alcohol. The optical microscope (OM) was usually used to observe the metallographic structure of the alloy and calculate the grain size of the alloy by the linear intercept method. The second phase composition and morphology were analyzed by scanning electron microscope (SEM, TESCAN VEGA II LMU) and energy spectrometer (EDS, OXFORD INCA Energy 350). The field emission electron probe micro-analyzer (FE-EPMA, JXA-8100) was used to characterize the distribution of solution elements and analyze micro-area

Table 1 Chemical composition of Mg-8Zn-1Mn-3Sn-*x*Gd alloys (wt%)

x	Zn	Mn	Sn	Gd	Mg
0	8	1	3	0	Bal.
0.5	8	1	3	0.5	Bal.
0.8	8	1	3	0.8	Bal.
1.2	8	1	3	1.2	Bal.

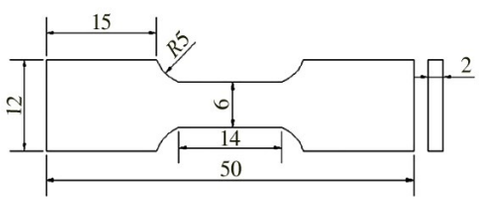

Fig.1 Sketch map of tension specimen

components. The phase identification was characterized by X-ray diffractometer (XRD, D/MAX-2500PC) with a scanning speed of 1°/min. The differential scanning calorimeter (DSC, METTLERTGA DSC I/1100LF) was used to analyze the formation process of each second phase during solidification.

2 Results and Discussion

2.1 Microstructure

Fig. 2 shows the metallographic microstructure of as-cast Mg-8Zn-1Mn-3Sn-*x*Gd alloys. According to Fig. 2a, it can be seen that the Mg-8Zn-1Mn-3Sn alloy is composed of α-Mg dendrites and eutectic compounds in the interdendritic region. According to the grain size diagram (Fig. 2e), the average grain size of the alloy is 50.47 μm, and most of the grain sizes are concentrated in 45~65 μm. When x=0.5, the coarse dendrites are refined, and the number of second phases at the grain boundaries increases significantly (Fig. 2b). The average grain size of the alloy is 35.24 μm, and most of the grain sizes are concentrated in 30~40 μm (Fig. 2f). As the Gd content increases from 0.8wt% to 1.2wt% , the dendrite structure becomes more obvious (Fig. 2c and 2d). The average grain size of the alloy in Fig. 2g and 2h is 32.68 and 29.74 μm according to the linear intercept method, respectively. After adding Gd to the alloy, the grain size of the alloy is significantly reduced, indicating that the Gd element can refine the grain. The reasons are as follows. (1) The equilibrium distribution coefficient of the Gd in Mg is less than 1. During the solidification process, solute atoms are enriched at the front of the solid-liquid interface of dendrite growth, forming a solute-rich region. The growth of dendritic requires continuous acquisition of atoms from the liquid phase, and the formation of solute-rich regions can hinder the diffusion of solute atoms from the distant liquid phase to the front of the solid-liquid interface. Therefore, it can effectively inhibit the growth of α-Mg matrix. (2) With the addition of Gd, a new second phase is formed, which changes the solidification process of the alloy and hinders the growth of

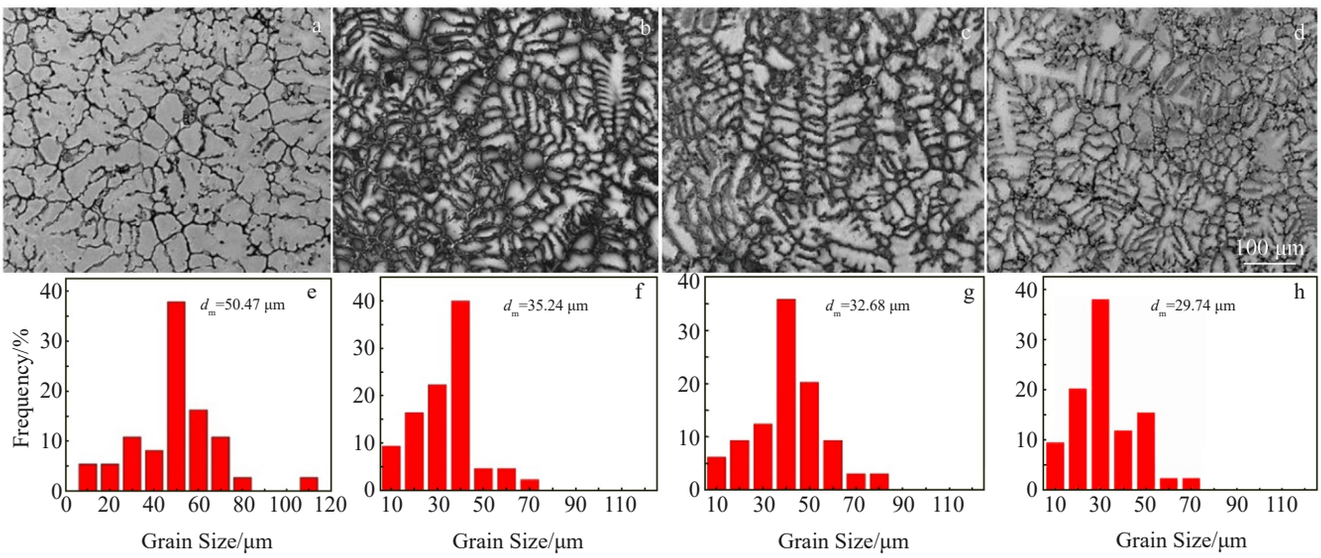

Fig.2 Metallographic microstructure (a~d) and corresponding grain size distribution (e~f) of the as-cast Mg-8Zn-1Mn-3Sn-*x*Gd alloy: (a, e) *x*=0, (b, f) *x*=0.5 , (c, g) *x*=0.8, and (d, h) *x*=1.2

crystal grains.

2.2 Phase composition of the alloy

Fig. 3 shows the XRD patterns of Mg-8Zn-1Mn-3Sn-*x*Gd alloy. When *x*=0, the alloy is composed of α-Mg matrix, $MgZn_2$, MgZn, Mg_7Zn_3, and Mg_2Sn phase, which is further confirmed by the EDS results. When the Gd element is added, a new diffraction peak appears in the spectrum, indicating the appearance of a new second phase in the alloy. Combined with the EDS result, the new phase is determined to be the MgSnGd ternary phase[21]. As the Gd content increases, the intensity of the new diffraction peak gradually increases. When *x*=1.2, the intensity of the new diffraction peak reaches the highest. It means that the quantity of the MgSnGd phase is the largest compared to other alloys. At the same time, the diffraction peak intensity of Mg_2Sn phase decreases. The reason is that Gd atoms and Sn atoms are enriched in the liquid region at the front of the solidification interface during the solidification process. As the temperature decreases, the grains keep growing, and the concentration of Gd and Sn atoms before the solidification interface continues to increase.

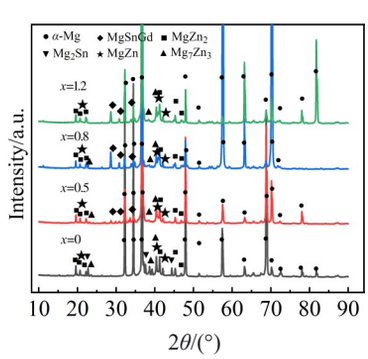

Fig.3 XRD patterns of as-cast Mg-8Zn-1Mn-3Sn-*x*Gd alloys

Before the binary eutectic reaction (L→α-Mg+Mg_2Sn), the MgSnGd phase is formed firstly, which consumes a large amount of Sn element and reduces the quantity of the Mg_2Sn phase.

Fig. 4a shows that the second phase in the Mg-8Zn-1Mn-3Sn alloy is mainly distributed near the grain boundary, which is a semi-continuous network structure. There are three different contrast compounds in the interdendritic region. According to the EDS results of region A, the atomic ratio of Mg:Zn is close to 7:3; combined with XRD results, it can be determined that the phase is Mg_7Zn_3 (Fig. 5a). For region B, the atomic ratio of Mg:Zn is close to 1:1, and this phase can be identified as MgZn (Fig.5b). For region C, the atomic ratio of Mg:Sn is close to 2:1, and the phase can be identified as Mg_2Sn (Fig. 5c). The addition of Gd element makes a new second phase appear in the alloy. According to the results of EDS (Fig.5d), the atomic ratio of Mg:Sn:Gd is close to 1:1:1. Combined with the XRD pattern, it can be determined as MgSnGd.

When 0.5wt% Gd is added, MgSnGd phase is formed in the grain and grain boundary, and the morphology of the semi-continuous network second phase begins to change. As the Gd content increases to 0.8wt%, the number of MgSnGd phase in the alloy increases significantly, and the Mg_7Zn_3 phase at the grain boundary changes from a semi-continuous network to a discontinuous network. As the Gd content increases to 1.2wt% , the Mg_7Zn_3 phase at the grain boundary is significantly refined, and there is a phenomenon of MgSnGd phase aggregation in some areas. The reason for this phenomenon is that Gd and Sn atoms are enriched in the liquid phase area at the front of the solidification interface during the solidification process, resulting in constitutional supercooling. As the Gd content further increases to 1.2wt% , the Gd atoms enriched in the liquid region will further increase, resulting in an increase of the supercooling degree. The increase of the

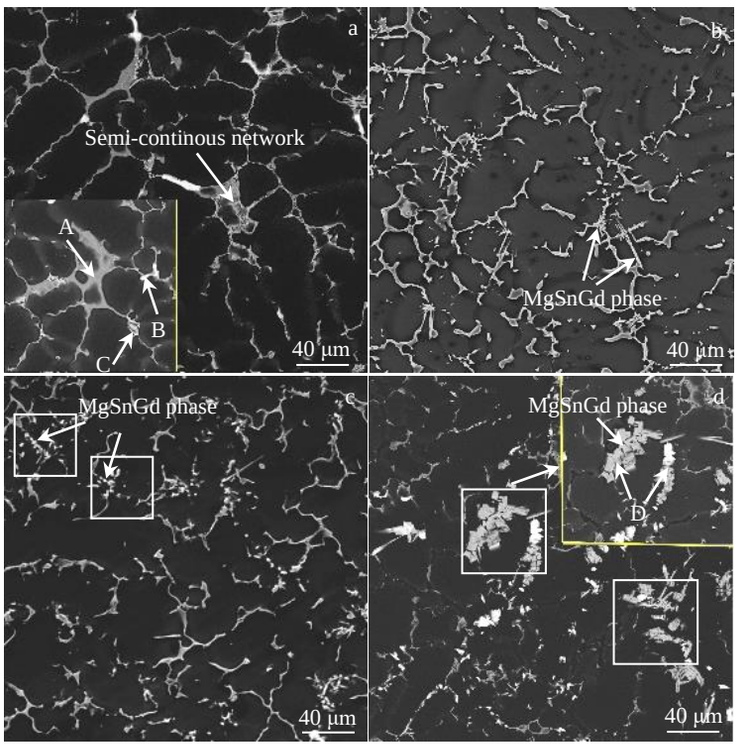

Fig.4 SEM images of as-cast Mg-8Zn-1Mn-3Sn-*x*Gd alloys: (a) *x*=0, (b) *x*=0.5, (c) *x*=0.8, and (d) *x*=1.2

supercooling degree increases the growth rate of the MgSnGd phase which is first formed during the solidification process. The increase of the growth rate of MgSnGd phase leads to shorter diffusion time of Sn and Gd atoms. Therefore, the Sn and Gd atoms (shorter diffusion time) and Mg atoms combine in part region of the alloy and continue to nucleate and grow. At the same time, the MgSnGd phase is pushed to the growth interface, hindering the growth of dendrites, so that the dendrites structure is refined. However, neither XRD nor EDS detected the presence of Mn element. According to Ref. [22], most of the Mn element is solid-dissolved in the Mg matrix, only a small part of α-Mn exists in the Mg matrix, and the amount of Mn added in the alloy is small (0.65wt%), so no Mn element is detected.

2.3 Phase formation and solidification paths

According to Fig.6 and Table 2, it can be seen that the DSC curve of Mg-8Zn-1Mn-3Sn-*x*Gd alloys has five exothermic peaks in the range of 100~700 °C, and the temperature of peak 1 is about 340 °C, which corresponds to the eutectic temperature of Mg_7Zn_3[23], the corresponding phase transition reaction is L→α-Mg+Mg_7Zn_3. The temperature of peak 2 is about 370 °C, which is corresponding to the phase transition temperature of $MgZn_2$, and the phase transition reaction is L→α-Mg+$MgZn_2$. The temperature of peak 3 is about 410 °C, which is corresponding to the phase transition temperature of MgZn. The temperature of peak 4 is about 550 °C, which is corresponding to the phase transition temperature of Mg_2Sn, and the phase transition reaction is L→α-Mg+Mg_2Sn. The temperature of peak 5 is about 610 °C, corresponding to the melting peak of α-Mg. In general, the difficulty of forming compounds between elements can be judged by the difference in electronegativity. The greater the difference in electronegativity, the greater the bonding force between atoms, and the easier it is to form intermetallic compounds. The electronegativity value of each element of Mg-8Zn-1Mn-3Sn magnesium alloy is shown in Table 3. The difference in electronegativity between Mg and Sn is the largest for Mg-8Zn-1Mn-3Sn alloy. At the same time, Mg_2Sn (770 °C) is a high temperature phase, which may be formed firstly during the solidification process.

After adding Gd to the Mg-8Zn-1Mn-3Sn alloy, the positions of the exothermic peaks are basically unchanged, and second phases such as Zn-Gd, Sn-Gd and Mg-Zn-Gd may be formed in the alloy (according to Table 3). However, combining the XRD and EDS results (Fig. 3 and Fig. 5), no secondary phases such as Mg-Gd, Sn-Gd and Zn-Gd are found in the alloy. A new exothermic peak appears in the alloy, the peak temperature is 630 ℃, and combining XRD and EDS results, the peak may correspond to the phase transition temperature of MgSnGd phase.

The formation enthalpy of alloy (ΔH) can be used to indicate the difficulty of the formation of intermetallic compounds. The smaller the value, the easier the formation of intermetallic compounds. According to Ref. [24], the formation enthalpy of Mg_7Zn_3, $MgZn_2$, and Mg_2Sn is −3.5, −12.95, and −18.90 kJ/mol, respectively. Therefore, the result of Fig. 6a is confirmed from the perspective of thermodynamics. Meanwhile, based on the Miedema extended

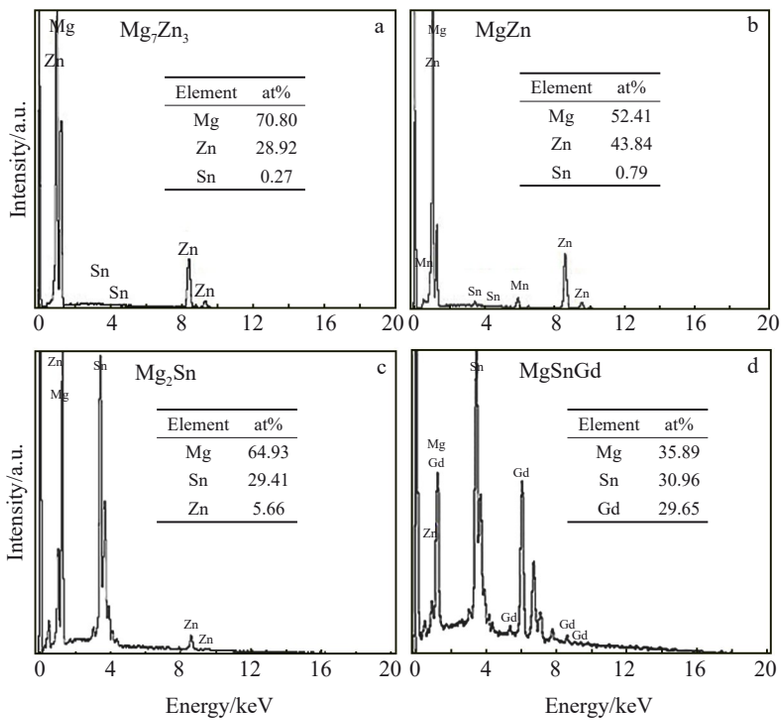

Fig.5 EDS results of regions A~C marked in Fig.4a (a~c) and region D marked in Fig.4d (d) for as-cast Mg-8Zn-1Mn-3Sn-*x*Gd alloys

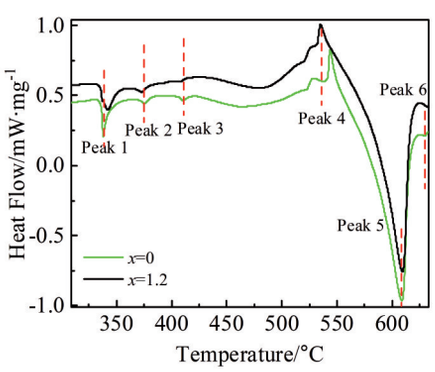

Fig.6 DSC curves of Mg-8Zn-1Mn-3Sn-*x*Gd alloys

Table 2 Exothermic peak temperature in Fig. 6 for the as-cast Mg-8Zn-1Mn-3Sn-*x*Gd alloy (°C)

x	Peak 1	Peak 2	Peak 3	Peak 4	Peak 5	Peak 6
x=0	340	373	408	548	608	-
x=1.2	337	376	410	550	609	630

Table 3 Electronegativity difference of as-cast Mg-8Zn-1Mn-3Sn alloy

Element	Electronegativity, E_i	$\|E_i-E_{Mg}\|$	$\|E_i-E_{Gd}\|$
Mg	1.31	-	0.11
Zn	1.65	0.34	0.45
Mn	1.55	0.24	0.35
Sn	1.96	0.65	0.76
Gd	1.20	0.11	-

model[25], the formation enthalpy of ternary compounds can be calculated. It is calculated that the formation enthalpy of MgSnGd is −50.1 kJ/mol, which is much lower than that of other phases. Therefore, it can be judged that the MgSnGd phase is most easily formed in the alloy. At the same time, since the MgSnGd phase is a high-temperature phase, its melting point is 1100 °C[26]. Combined with the results of peak 6 in Fig. 6, it shows that the MgSnGd phase first nucleates during the solidification process, which is consistent with the results of related studies[27,28]. Since the Gd element has a large solid solubility in the Mg matrix, most of the Gd atoms are dissolved in the Mg matrix, and only a small part of the Gd atoms are precipitated to form the second phase during the solidification process. Therefore, the addition of Gd to magnesium alloys is generally used as solid solution strengthening. However, when the temperature is 630 °C, the α-Mg in the melt does not start to nucleate, and the elements still exist in the melt in a free state, which provides a large amount of Sn and Gd atoms for the formation of MgSnGd phase. Therefore, adding minor Gd element to the alloy can also form the second phase to strengthen the matrix. At the same time, the formation of MgSnGd phase can also inhibit the formation of the second phases such as Zn-Gd, Sn-Gd and Mg-Zn-Gd.

Fig. 7 shows the EPMA mapping results of the Mg-8Zn-1Mn-3Sn-*x*Gd alloy. It can be seen that the Zn element is mainly concentrated near the grain boundary. Combining the results of SEM and EDS, it is found that the compound at the grain boundary is mainly Mg_7Zn_3. The morphology of the Mg_7Zn_3 is a semi-continuous network (Fig. 7b and 7c). The

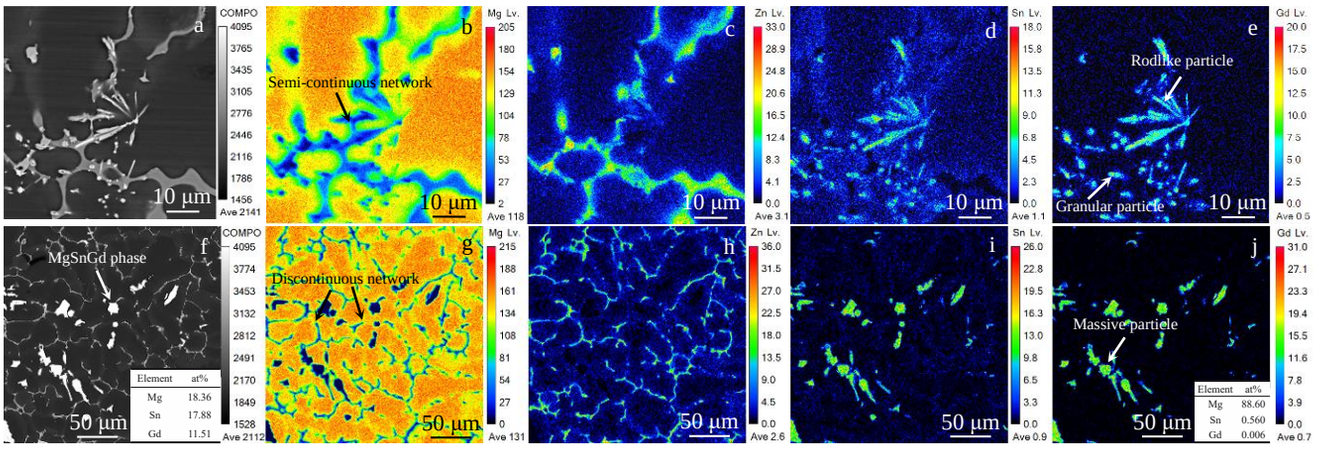

Fig.7 Microstructure and EPMA mapping results of Mg, Zn, Sn, Gd element for as-cast Mg-8Zn-1Mn-3Sn-0.5wt%Gd (a~e) and Mg-8Zn-1Mn-3Sn-1.2wt%Gd (f~j)

new second phase which is composed of Mg, Sn and Gd element in the alloy can be seen from the EPMA spectrogram (Fig. 7f), which further verifies that it is MgSnGd. When the Gd content increases from 0.5wt% to 1.2wt%, the morphology of MgSnGd phase changes from granular to massive (Fig. 7e and 7j), and the Mg_7Zn_3 phase at the grain boundary changes from a semi-continuous network to a discontinuous network (Fig. 7b and 7g). The reason for the change of morphology is that the nucleation temperature (630 °C) of MgSnGd phase is higher than the liquidus temperature (610 °C), which causes the MgSnGd phase form firstly during the solidification process (L→L+MgSnGd). The MgSnGd phase formed firstly at the grain boundary hinders the continuous growth of the Mg_7Zn_3 eutectic phase which forms later. Studies have shown that the second phase having a coherent relationship with α-Mg is an important condition for the heterogeneous nucleation core of α-Mg matrix crystal grains. According to the edge-edge matching model[29], whether the second phase and the matrix phase have a coherent relationship can be determined by the value of mismatch (V_{cp}) of the close-packed plane (CP) spacing between the two phases and the value of interatomic misfit on close-packed row (CR). When the value of plane mismatch is less than 6%, and the value of interatomic misfit corresponding to the close-packed direction on the close-packed plane is less than 10%, there is a possible coherent relationship between the second phase and the matrix phase. The interplanar spacing misfits are defined as follows:

$$f_d = \frac{|d_M - d_P|}{d_P} \quad (1)$$

where d is the interplanar spacing, and subscript "M" and "P" mean the matrix phase (Mg) and precipitated phase (MgSnGd), respectively. Magnesium has a hexagonal close-packed structure (hcp). According to the PDF-4+2020 card library, its close-packed and sub-close-packed faces are (0002), (10$\bar{1}$1), (10$\bar{1}$0), and the corresponding crystal plane spacings are 0.26, 0.245, and 0.277 nm, respectively. The MgSnGd phase has a tetragonal structure (I4), its close-packed and sub-closed faces are (004), (110), and (114), and the corresponding interplanar spacings are 0.396, 0.310, and 0.244 nm, respectively. The calculated mismatch of α-Mg and MgSnGd close-packed crystal planes and sub-closed crystal planes is shown in Table 4. According to the calculation results of plane matching and crystal orientation matching, the required orientation relationship can be obtained: (1) (0002) Mg//(114) MgSnGd: [11$\bar{2}$0] Mg/[110] MgSnGd, (2) (10$\bar{1}$1) Mg//(114) MgSnGd: [10$\bar{1}$0] Mg/[110] MgSnGd.

The results show that there are two possible pairs of coherent orientation relationships between α-Mg and MgSnGd. The interatomic mismatch is defined as follows:

$$f_r = \frac{|r_M - r_P|}{r_P} \quad (2)$$

where r is the interatomic distance, and subscript "M" and "P" mean the matrix phase (Mg) and precipitated phase (MgSnGd), respectively. Since magnesium has a hexagonal close-packed structure (hcp), its close-packed direction and sub-close packed direction are [1120], [10$\bar{1}$0], [11$\bar{2}$3], and the lattice constants a, b, and c are 0.3202, 0.3202, 0.5199 nm, respectively. According to the Ref.[30, 31], the lattice constant can be used to indicate the atomic distance in the corresponding crystal direction. For the hexagonal close packed structure (hcp), the corresponding interatomic distance in the close packed direction [11$\bar{2}$0] and the sub-close packed direction [10$\bar{1}$0] is defined as follows:

$$r_H = a_H \quad (3)$$

Table 4 Matching plane pairs between α-Mg and MgSnGd

Potential matching plane	V_{cp}/%	Potential matching plane	V_{cp}/%
(0002)//(004)	52.40	(10$\bar{1}$1)//(004)	61.70
(0002)//(110)	19.03	(10$\bar{1}$1)//(110)	6.67
(0002)//(114)	6.02	(10$\bar{1}$1)//(114)	0.27
(10$\bar{1}$0)//(004)	43.60	(10$\bar{1}$0)//(110)	12.03
(10$\bar{1}$0)//(114)	11.79	-	-

$$r_H = \frac{\sqrt{3}}{2} a_H \quad (4)$$

where r is the atomic distance, a is the lattice constant and subscript "H" represents the close-packed hexagonal structure. For the tetragonal structure (I4), the corresponding atomic distance on the crystal orientation [110] is defined as follows:

$$r_I = \frac{\sqrt{2}}{2} a_I \quad (5)$$

where r is the atomic distance, a is the lattice constant and I represents the tetragonal structure. The lattice constants a, b, and c of the MgSnGd phase are 0.4389, 0.4389, and 1.5851 nm, respectively. According to the corresponding calculation results, the interatomic mismatch of (0002) Mg//(114) MgSnGd: $[11\bar{2}0]$ Mg/[110] MgSnGd is 3.19% (<10%), which matches the edge-edge matching model. The interatomic mismatch of $(10\bar{1}1)$ Mg//(114) MgSnGd: $[10\bar{1}0]$ Mg/[110] MgSnGd is 10.63% (>10%), which does not match the edge-edge matching model. Therefore, there is only a pair of coherent orientation relationship between α-Mg and MgSnGd phase. From the perspective of the crystallographic, it is shown that the MgSnGd formed firstly during the solidification process can be used as the heterogeneous nucleation core of α-Mg (formed later) to refine the grain.

When the Gd content is 0.5wt%, the MgSnGd phase is mainly granular structure, and a small part is rodlike structure (Fig. 7e). Since the MgSnGd phase is a tetragonal crystal system whose different crystal planes have different adsorption capacities for atoms, the crystal plane with high index has higher energy and strong adsorption capacity. Therefore, high index crystal plane (the growth plane) has more solute atoms, resulting in faster growth rate perpendicular to the high index crystal plane, and the MgSnGd phase can grow into a rodlike structure.

When the Gd content is 1.2wt%, the MgSnGd phase is mainly massive structure. The reason is that when the Gd content increases from 0.5wt% to 1.2wt%, the Gd atom concentration at the front of the solid-liquid interface increases, which provides enough atoms for the continuous growth of the MgSnGd phase, so they grow into a massive structure (Fig. 7j). According to Fig. 7d, 7i, 7e, and 7j, with the increase of Gd content, the concentration of Sn and Gd atoms in the α-Mg matrix decreases significantly. This is because when the Gd content is 0.5wt%, the MgSnGd phase formed firstly during the solidification process has a small amount of nucleation and a slower growth rate, and Sn and Gd atoms in the melt are only partially consumed. Therefore, the rest of the Sn and Gd atoms will still be dissolved in the α-Mg matrix which forms later. When the Gd content is 1.2wt%, the Gd atom concentration further increases, resulting in an increase of the subcooling degree. The growth rate of the MgSnGd phase is increased owing to an increase of the supercooling degree, and the MgSnGd phase can grow continuously and rapidly, which causes the consumption of a large amount of Sn and Gd atoms, resulting in a significant decrease in the concentration of Sn and Gd atoms in the α-Mg matrix.

2.4 Mechanical properties

The tensile curve of Mg-8Zn-1Mn-3Sn-xGd is shown in Fig. 8, which shows that the mechanical properties of alloys with Gd addition are higher than those of Mg-8Zn-1Mn-3Sn alloy. It can be seen that the addition of Gd to the Mg-8Zn-1Mn-3Sn alloy has a positive strengthening effect, especially in tensile strength. According to Table 5, the tensile strength, yield strength and elongation of Mg-8Zn-1Mn-3Sn alloy are 101±7 MPa, 87.5±0.5 MPa, 1.25%±0.55%, respectively. When 0.5wt% Gd is added, the tensile strength, yield strength, and elongation of the alloy are 207.5±2.5 MPa, 135±1 MPa, and 4%±0.2%, respectively. Compared with Mg-8Zn-1Mn-3Sn alloy, its comprehensive mechanical properties are greatly improved. The reasons for the improvement of mechanical properties include several aspects. (1) According to the grain size diagram (Fig. 2e~2h), the addition of Gd element refines the grains size of the alloy, and the refinement of the grains greatly increases the grain boundary area, which effectively hinders the sliding of crystal plane. (2) According to Fig. 4a, the semi-continuous network Mg_7Zn_3 phase (brittle second phase) at the grain boundary will separate the Mg matrix, which makes it easy to produce stress concentration at the grain boundary during the alloy deformation process. As a result, the Mg_7Zn_3 phase is likely to become the source of crack initiation and crack along the grain boundary, thereby reducing the mechanical properties of the alloy. The formation of MgSnGd phase changes the microstructure morphology of the alloy, transforms the eutectic phase from a semi-continuous network to a discontinuous network, reduces the negative effect of semi-continuous network phase, and improves the plasticity of the alloy (Fig. 4b and 4c). (3) The granular MgSnGd phase is evenly distributed in the matrix, which pins the dislocations and effectively hinders the

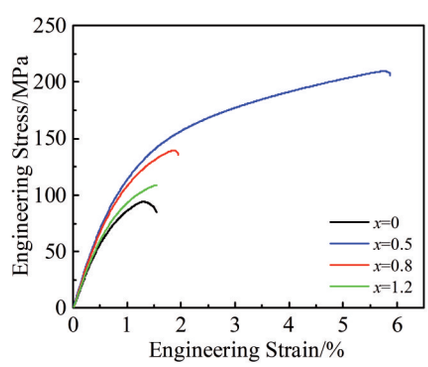

Fig.8 Tensile engineering stress-strain curves of as-cast Mg-8Zn-1Mn-3Sn-xGd alloys

Table 5 Mechanical properties of Mg-8Zn-1Mn-3Sn-xGd alloys

x	Tensile strength/MPa	Yield strength/MPa	Elongation/%
0	101±7	87.5±0.5	1.25±0.55
0.5	207.5±2.5	135±1	4±0.2
0.8	137.5±2.5	111±5	1±0.2
1.2	104±4	91±1	0.5±0.1

movement of the dislocations, thereby strengthening the alloy.

As the Gd content increases from 0.5wt% to 0.8wt%, the grain size of the alloy decreases further, but the growth and aggregation of MgSnGd phase appear in some areas of the alloy (Fig. 4c). The negative effect of MgSnGd phase aggregation and growth on the mechanical properties of the alloy is greater than the grain refinement, which causes the decrease of the mechanical properties of the alloy. When the Gd content is 1.2wt%, the tensile strength and yield strength of the alloy increase less than those of Mg-8Zn-1Mn-3Sn, and the elongation decreases. The reason is that as the Gd content increases, the granular MgSnGd phase accumulates and grows in some areas (Fig. 4d), which greatly deteriorates the mechanical properties of the alloy, especially the elongation.

3 Conclusions

1) The addition of minor Gd element can not only refine grains of the Mg-8Zn-1Mg-3Sn alloy, but also change the solidification process, which leads to the transformation of semi-continuous network Mg_7Zn_3 phase at the grain boundary into a discontinuous network.

2) The MgSnGd phase formed firstly in the solidification process consumes a large amount of Sn and Gd elements, which reduce the content of Mg_2Sn and inhibit the formation of Sn-Gd and Mg-Zn-Gd phases. The MgSnGd phase can be used as the core of α-Mg heterogeneous nucleation to refine grains.

3) When the Gd content is 0.5wt%, the comprehensive mechanical properties of the alloy are the best, and the tensile strength, yield strength, and elongation are 207.5 MPa, 135 MPa, and 4%, respectively. The significant improvement of the mechanical properties of the alloy is due to the grain refinement and precipitation strengthening.

References

1 Yang Mingbo, Zhu Yi, Liang Xiaofeng *et al. Materials Science and Engineering A*[J], 2011, 528(3): 1721

2 Shi Binqing, Chen Rongshi, Ke Wei. *Transactions of Nonferrous Metals Society of China*[J], 2010, 20: 341

3 Cong Mengqi, Li Ziquan, Liu Jinsong *et al. Russian Journal of Non-Ferrous Metals*[J], 2016, 57(5): 445

4 Yang Mingbo, Hou Mengdan, Zhang Jia *et al. Transactions of Nonferrous Metals Society of China*[J], 2014, 24(8): 2497

5 Chen Xia, Zhang Dingfei, Xu Junyao *et al. Journal of Alloys and Compounds*[J], 2021, 850

6 Nie Jianfeng. *Metallurgical and Materials Transactions A*[J], 2012, 43(11): 3891

7 Chen X, Zhang D F, Feng J K *et al. Rare Metal Materials and Engineering*[J], 2020, 49(9): 2920

8 Chen R, Xu J Y, Zhang D F *et al. Rare Metal Materials and Engineering*[J], 2019, 48(7): 2084

9 Liu Peng, Jiang Haitao, Cai Zhengxu *et al. Journal of Magnesium and Alloys*[J], 2016, 4(3): 188

10 Zhang Dingfei, Qi Fugang, Lan Wei *et al. Transactions of Nonferrous Metals Society of China*[J], 2011, 21(4): 703

11 Qi Fugang, Zhang Dingfei, Zhang Xiaohua *et al. Transactions of Nonferrous Metals Society of China*[J], 2014, 24(5): 1352

12 Zhang Dingfei, Shi Guoliang, Dai Qingwei *et al. Transactions of Nonferrous Metals Society of China*[J], 2008, 18: 59

13 Zhang Yuan, Li Jianxing, Li Jingyuan. *Journal of Alloys and Compounds*[J], 2018, 730: 458

14 Zhao Yang, Zhang Dingfei, Feng Jingkai *et al. Journal of Materials Research and Technology*[J], 2020, 9(4): 8834

15 Xu Yuling, Gensch Felix, Ren Zhen *et al. Progress in Natural Science: Materials International*[J], 2018, 28(6): 724

16 Huang Hua, Miao Hongwei, Yuan Guangyin *et al. Journal of Materials Research and Technology*[J], 2018, 7(2): 135

17 Wang Dan, Fu Penghuai, Peng Liming *et al. Materials Characterization*[J], 2019, 153: 157

18 Hu Guangshan, Xing Bo, Huang Fengli *et al. Journal of Alloys and Compounds*[J], 2016, 689: 326

19 Hu Guangshan, Zhang Dingfei, Tang Tian *et al. Materials Science and Engineering A*[J], 2015, 634: 5

20 Zhao Yang, Zhang Dingfei, Lei Renjie *et al. Journal of Materials Research and Technology*[J], 2020, 9(6): 12 737

21 Lemoine P, Lee-Hone N R, Ryan D H *et al. Physical Review B* [J], 2014, 89(17): 174 428

22 Hou Caihong, Qi Fugang, Ye Zhisong *et al. Materials Science and Engineering A*[J], 2020, 774(2): 138 933

23 Wu Xiaofeng, Xu Chunxiang, Zhang Zhengwei *et al. Advanced Engineering Materials*[J], 2020, 22(3): 1 900 964

24 Hu G, Xing B, Huang F *et al. Materials Science and Technology* [J], 2016, 33(3): 294

25 Ouyang Yifang, Zhong Xiaping, Du Yong *et al. Journal of Alloys and Compounds*[J], 2006, 416(1-2): 148

26 Manfrinetti P, Provino A, Gschneidner K A. *Journal of Alloys and Compounds*[J], 2009, 482(1-2): 81

27 Kozlov A, Ohno M, Arroyave R *et al. Intermetallics*[J], 2008, 16(2): 299

28 Muthuraja C, Akalya A, Ahmed R Raseem *et al. Journal of Alloys and Compounds*[J], 2017, 695: 3559

29 Zhang M, Kelly P, Easton M *et al. Acta Materialia*[J], 2005, 53(5): 1427

30 Zhang M X, Kelly P M. *Acta Materialia*[J], 2005, 53(4): 1073

31 Zhang M X, Kelly P M. *Acta Materialia*[J], 2005, 53(4): 1085

微量Gd添加对Mg-8Zn-1Mn-3Sn合金组织转变及性能的影响

薛寒松[1,2]，周　扬[1]，李　鹤[1]，王金阳[1]，刘　松[1]，张丁非[2]

(1. 重庆大学 材料科学与工程学院，重庆 400044)

(2. 重庆大学 国家镁合金材料工程技术研究中心，重庆 400044)

摘　要：研究了微量Gd的添加对Mg-8Zn-1Mn-3Sn合金显微组织及性能的影响。结果表明，Mg-8Zn-1Mn-3Sn-*x*Gd主要由*α*-Mg基体、$MgZn_2$、Mg_7Zn_3、Mg_2Sn相、MgSnGd相组成。MgSnGd相为高温相，在合金凝固过程中最先形成，改变了凝固过程，使晶界处半连续第二相转变为断网状。MgSnGd相与*α*-Mg基体存在共格位向关系，能作为异质形核核心细化合金晶粒。Mg-8Zn-1Mn-3Sn-0.5Gd合金的综合力学性能最佳，合金力学性能得到显著提高的机制为通过添加Gd元素细化晶粒组织、MgSnGd相钉扎晶界阻碍位错运动以及晶界第二相形貌转变。

关键词：Mg-Zn-Mn-Sn合金；MgSnGd相；晶粒细化；力学性能；Gd添加

作者简介：薛寒松，男，1968年生，博士，副教授，重庆大学材料科学与工程学院，重庆 400044，电话：023-65111212，E-mail：hsxue@sohu.com